JOURNAL OF SPACECRAFT AND ROCKETS
Vol. 42, No. 2, March–April 2005

Calculation of Shock Wave Structure over Power Law Bodies in Hypersonic Flow

Wilson F. N. Santos*
National Institute for Space Research, Cachoeira Paulista-SP, 12630-000, Brazil
and
Mark J. Lewis†
University of Maryland, College Park, Maryland 20742

A numerical study is conducted of power law shaped leading edges situated in a rarefied hypersonic flow. The motivation is interest in investigating the flowfield structure of power law shaped leading edges as possible candidates for blunting geometries of hypersonic leading edges. The primary aim is to examine in detail the effect of geometry of such leading edges on the shock wave structure. The sensitivity of the shock wave shape, standoff distance, and shock wave thickness to shape variations of the power law class of leading edges is calculated by using the direct simulation Monte Carlo method. Calculations show that the shape of the shock wave is in agreement with that predicted by the analytic hypersonic small disturbance theory for the flow conditions considered.

Nomenclature

A, B	=	constant in power law shock equation (2)
a	=	constant in power law body equation (1)
c	=	speed of sound, m/s
H	=	body height at the base, m
Kn	=	Knudsen number, λ/l
L	=	body length, m
l	=	characteristic length, m
M	=	Mach number, V/c
m	=	shock wave power law exponent
n	=	body power law exponent
R_c	=	radius of curvature, m
Re	=	Reynolds number, $\rho V l/\mu$
s	=	arc length, m
V	=	velocity, m/s
v	=	velocity component in the η direction, m/s
x, y	=	Cartesian axes in physical space, m
β	=	shock wave angle, deg
Δ	=	shock wave standoff distance, m
δ	=	shock wave thickness, m
η	=	coordinate normal to body surface, m
θ	=	wedge half angle, body slope angle, deg
λ	=	mean free path, m
ξ	=	coordinate tangent to body surface, m
ρ	=	density, kg/m^3
τ	=	characteristic shock slope
Ω	=	vorticity, s^{-1}

Subscripts

w	=	wall conditions
0	=	stagnation conditions
2	=	conditions behind the shock wave
∞	=	freestream conditions

Presented as Paper 2003-1134 at the 41st Aerospace Sciences Meeting, Reno, NV, 6–9 January 2003; received 6 October 2003; revision received 16 March 2004; accepted for publication 5 April 2004.

*Researcher, Combustion and Propulsion Laboratory. Member AIAA.
†Professor, Aerospace Engineering Department. Associate Fellow AIAA.

Introduction

WITH the recent interest in hypervelocity flight, the effort to design efficient hypersonic flight vehicles, which depend on high-lift, low-drag configurations, has focused some attention on the waverider concept pioneered by Nonweiler.[1] The waverider concept is one class of aerospace vehicle that has shown the ability to attain high lift-to-drag ratio compared to more conventional designs. Waveriders are designed analytically with infinitely sharp leading edges for shock wave attachment. The shock wave acts as a barrier to prevent spillage of higher pressure airflow from the lower side of the vehicle to the upper side, resulting in a high-pressure differential and enhanced lift. Because any practical waverider will have some degree of leading-edge bluntness for heat transfer, manufacturing, and handling concerns, the predicted performance of these configurations may not be achieved. Moreover, because of the viscous effects, the shock wave will be detached from the leading edge, and hence, the aerodynamic performance of the vehicle may be degraded from ideal performance. In this context, power law shaped leading edges ($y \propto x^n, 0 < n < 1$) may provide the required bluntness for heat transfer, manufacturing, and handling concerns with reduced departures from ideal aerodynamic performance. This concept is based on work available in the literature that pointed out, based on Newtonian flow analysis, that these shapes exhibit both blunt and sharp aerodynamic properties.

A great deal of experimental and theoretical work has been carried out previously on power law forms representing blunt geometries. The major interest in these theoretical works has been finding solutions to the hypersonic small disturbance form of the inviscid adiabatic-flow equations. The equations of motion for hypersonic flow over slender bodies can be reduced to simpler form by incorporating the hypersonic slender-body approximations.[2]

Lees and Kubota[3] observed that similarity exists for hypersonic flows whenever the shock shape follows a power law variation with the streamwise distance, provided the hypersonic slender-body equations are considered in the limit as $(M_\infty \tau)^{-2} \to 0$, where M_∞ is the freestream Mach number and τ is a characteristic shock slope. According to their work, energy considerations combined with a detailed study of the equations of motion show that flow similarity is possible for a class of bodies of the form x^n, provided that $\frac{2}{3} < n < 1$ for a two-dimensional body and $\frac{1}{2} < n < 1$ for an axisymmetric body. The similarity solutions referred herein are solutions for self-similar flows, that is, flows in which the flowfield between the shock wave and the body can be expressed in terms of functions that, in suitable coordinates, are independent of one of the coordinate directions.

Freeman et al.[4] and Beavers[5] have studied experimentally the hypersonic flow on axisymmetric power law bodies. They have

presented detailed shock shape data for a series of power law bodies and registered some disagreement with other experimental results in the literature. Information on the flowfield and shock wave shapes over plane power law bodies has been reported by Hornung[6] for $n = \frac{1}{2}$ and $\frac{2}{8}$. His theoretical solutions are based on the expansion scheme at large distance downstream of the nose of the bodies and large M_∞.

Mason and Lee[7] pointed that, for certain exponents, power law shapes exhibit aerodynamic properties similar to geometrically sharp shapes. They suggested the possibility of a difference between shapes that are geometrically sharp and shapes that behave aerodynamically as if they were sharp, but are actually blunt. For values of $0 < n < \frac{1}{2}$, the leading-edge radius of curvature becomes infinite at the nose, a characteristic of a blunt shape; for values of $\frac{1}{2} < n < 1$, the leading-edge radius of curvature approaches zero at the nose, a characteristic of a sharp shape. Furthermore, for $\frac{2}{3} < n < 1$, their numerical investigation predicted that the derivative of the pressure coefficient with respect to the body coordinate dC_p/ds approaches $-\infty$ at $x = 0$, a characteristic of a sharp body. In this way, there is a class of body shapes given by $\frac{1}{2} < n < \frac{2}{3}$, for which the leading edge may behave aerodynamically as a blunt body, even though the leading-edge radius of curvature is zero and another one given by $\frac{2}{3} < n < 1$ for which the leading edge may behave like an aerodynamically sharp body even though the leading-edge bluntness is infinite. Their analysis describes the details of the geometry and aerodynamics of low-drag axisymmetric bodies by using Newtonian theory. However, one of the important aspects of the problem, stagnation point heat transfer, was not considered.

By the consideration of two-dimensional rarefied hypersonic flow, the sensitivity of the pressure gradient and the stagnation point heating to shape variations of power law leading edges was investigated by Santos and Lewis[8] at zero angle of attack and by Santos and Lewis[9] at positive angles of attack. Through the use of direct simulation Monte Carlo (DSMC) method, they showed that the pressure gradient on the power law shapes is in agreement with that obtained by Mason and Lee[7] using Newtonian analysis. They also found that the stagnation point heating scales inversely with the square root of the radius or curvature for power law bodies that have finite radius of curvature.

Several experimental and theoretical studies have been devoted to the determination of the shock wave shape. From schlieren photographs obtained for flat plates in hypersonic flow, Vas et al.[10] found a power law shape with exponent of 0.49 offered the best fit on a flat plate with a square leading edge and a power law exponent of 0.50 provided the best fit for a flat plate with a round leading edge. McCarthy and Kubota[11] reported an experimental study of wakes behind a circular cylinder in supersonic flow and also found a power law shock wave shape with exponent of 0.516. Zapata et al.[12] studied high Mach number and low Reynolds number flow over a two-dimensional circular cylinder experimentally and identified best fits with power law shock wave exponents of 0.517 and 0.494 for an uncooled and a cooled model, respectively.

The primary goal of this paper is to investigate the effect of the power law exponent on the shock wave structure over such leading edges. The flow conditions represent those experienced by a vehicle at an altitude of 70 km. Therefore, the focus of the present study is the low-density region in the upper atmosphere, where numerical gas kinetic procedures are appropriate to simulate hypersonic flows. High-speed flows under low-density conditions deviate from perfect gas behavior because of the excitation of the internal modes of energy. At high altitudes, and, therefore, low density, the molecular collision rate is low and the energy exchange occurs under nonequilibrium conditions. Under these circumstances, the degree of molecular nonequilibrium is such that the Navier–Stokes equations are inappropriate. Alternatively, the DSMC method is used to examine the shock wave structure for the idealized situation of rarefied hypersonic two-dimensional flow. Attention will be focused on the analysis of the shape, thickness, and position of the shock wave relative to the body that produces it.

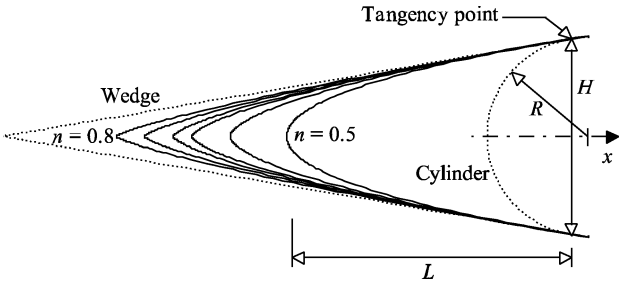

Fig. 1 Leading-edge geometries.

Leading-Edge Geometry Definition

In dimensional form, the body power law shapes are given by the following expression:

$$y = ax^n \tag{1}$$

where n is the power law exponent and a is the power law constant that is in turn a function of n.

The power-law shapes are modeled by assuming a sharp leading edge of half angle θ with a circular cylinder of radius R inscribed tangent to this wedge. The power law shapes, inscribed between the wedge and the cylinder, are also tangent to them at the same common point where they have the same slope angle. The circular cylinder diameter provides a reference for the amount of blunting desired on the leading edges. It is assumed that the leading-edge half angle is 10 deg and the circular cylinder diameter is 10^{-2}m. Solutions were done for values of power law exponents of $\frac{1}{2}$, 0.6, $\frac{2}{3}$, 0.7, $\frac{3}{4}$, and 0.8. Figure 1 shows this construction schematically for the set of investigated power law leading edges.

From geometric considerations, the power law constant a is obtained by matching the slope of the wedge, circular cylinder, and power law body at the point of tangency. The common body height H at the tangency point is equal to $2R\cos\theta$, and the body length L from the nose to the tangency point in the axis of symmetry is given by $nH/2\tan\theta$. Because the wake region behind the power law bodies is not of interest in this investigation, the power law bodies are modeled as infinitely long, but only the length L is considered. (It is assumed that the power law shape is a leading edge on a much larger vehicle surface.)

Computational Method and Procedure

A number of significant problems in fluid mechanics involve flows in the transitional regime, that is, flows for which the Knudsen number is larger than about 0.01 and less than about 10. The most successful numerical technique for modeling complex flows in the transitional regime has been the DSMC method developed by Bird.[13] The DSMC method models the flow as being a collection of discrete particles, each one with a position, velocity, and internal energy. The state of the particles is stored and modified with time as the particles move, collide, and undergo boundary interactions in simulated physical space.

A fundamental assumption in the DSMC method is that the gas is dilute, that is, the mean molecular diameter is much less than the mean molecular spacing of molecules in the gas. This feature of the DSMC method allows for the uncoupling of the molecular motion and collisions over the period of a specific time step. In this way, the predictions of the new positions of the molecules as well as the resulting boundary interactions are followed by the selection of a set of possible intermolecular collisions that are appropriate during the given time step. In general, the total simulation time, discretized into time steps, is identified with the physical time of the real flow, and the time step should be chosen to be sufficiently small in comparison with the local mean collision time.[14,15]

The variable hard sphere (VHS) molecular model[16] is utilized for the molecular potential. This model employs the simple hard sphere angular scattering law so that all directions are equally possible for postcollision velocity in the center-of-mass frame of reference.

However, the collision cross section depends on the relative speed of colliding molecules.

The energy exchange between kinetic and internal modes is controlled by the Borgnakke–Larsen statistical model.[17] The essential feature of this model is that a fraction of the collisions is treated as completely inelastic and the remainder of the molecular collisions is regarded as elastic. For the present study, the simulations are performed using a nonreacting gas model consisting of two chemical species, N_2 and O_2. The probability of an inelastic collision determines the rate at which energy is transferred between the translational and internal modes after an inelastic collision. For a given collision, the probabilities are designated by the inverse of the relaxation numbers, which correspond to the number of collisions necessary, on average, for a molecule to relax. Relaxation collision numbers of 5 and 50 were used for the calculations of rotation and vibration, respectively. The effective number of degrees of freedom in the partially excited vibrational states is calculated from the harmonic oscillator theory.

To implement the particle–particle collisions, the flowfield is divided into regions, which are subdivided into computational cells. The cell provides a convenient reference for the sampling of the macroscopic gas properties. The dimensions of the cells must be such that the change in flow properties across each cell is small. The linear dimensions of the cells should be small in comparison with the scale length of the macroscopic flow gradients normal to the streamwise directions, which means that the cell dimensions should be of the order of the local mean free path, or even smaller.[18,19] Each cell is further subdivided into four subcells, two subcells per cell in each direction. The collision partners are selected from the same subcell for the establishment of the collision rate. As a result, the flow resolution is much higher than the cell resolution.

The computational domain used for the calculations is chosen to be large enough so that the upstream and side boundaries can be specified as freestream conditions, where the incoming molecules are prescribed with undisturbed freestream velocity. Outgoing molecules across boundaries are discarded; the flow at the downstream outflow boundary is supersonic, and vacuum conditions are specified.[13] A schematic view of the computational domain is shown in Fig. 2. Flow symmetry is invoked to reduce the size of the computational domain.

The freestream and flow conditions used in the present calculations are those given by Santos[20] and summarized in Table 1, and the gas properties[13] are shown in Table 2. The freestream velocity V_∞ is assumed to be constant at 3.5 km/s, which corresponds to a freestream Mach number M_∞ of 12. The wall temperature T_w is defined as constant at 880 K. In addition, diffusion reflection with full thermal accommodation is assumed for the gas–surface interactions. This model implies that the particle translational and internal energies are distributed according to a Maxwellian distribution. The overall Knudsen number is defined as the ratio of the molecular mean free path in the freestream gas to a characteristic dimension of the flowfield. In the present study, the characteristic dimension was defined as being the diameter of the circular cylinder. Note that leading-edge radius could not be used for this definition because some of the shapes do not have a definable leading-edge radius. Hence, the freestream Knudsen number Kn_∞ is 0.0903 for all of the cases studied. Finally, the freestream Reynolds number per unit meter Re_∞ is 2.1455×10^4.

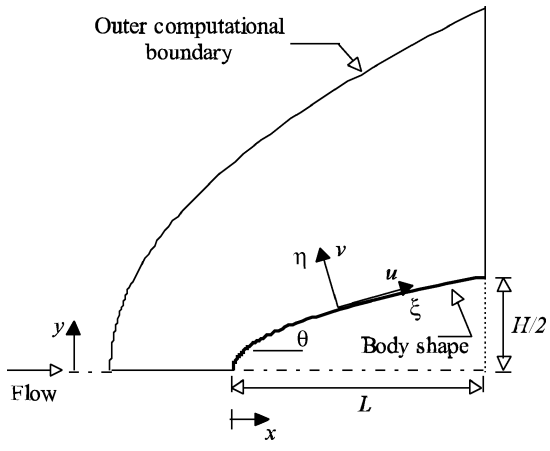

Fig. 2 Schematic of computational domain.

Table 1 Freestream and flow conditions

Parameter	Value	Unit
Temperature T_∞	220.0	K
Pressure p_∞	5.582	N/m^2
Density ρ_∞	8.753×10^{-5}	kg/m^3
Viscosity μ_∞	1.455×10^{-5}	Ns/m^2
Number density n_∞	1.8209×10^{21}	m^{-3}
Mean free path λ_∞	9.03×10^{-4}	m

Table 2 Gas properties

Parameter	O_2	N_2	Unit
Molecular mass	5.312×10^{-26}	4.65×10^{-26}	kg
Molecular diameter	4.010×10^{-10}	4.11×10^{-10}	m
Mole fraction	0.237	0.763	
Viscosity index	0.77	0.74	

Numerical accuracy in DSMC method depends on the chosen grid resolution as well as the number of particles per computational cell. Both effects were investigated to determine the number of cells and the number of particles required to achieve grid-independent solutions for the thermal nonequilibrium flow that arises near the leading edge. A discussion of both effects on the aerodynamic surface quantities is presented in the Appendix.

Computational Results and Discussion

Significant differences in the shock wave shape, shock wave thickness, and shock wave detachment distance were determined due to the variations in the body power law exponent.

Shock Wave Shape

The shock wave is generally regarded as a sudden discontinuity in an inviscid continuum flow, where the ratios of stream speed, density, pressure, and temperature across the shock wave are given by the classical Rankine–Hugoniot relations. In a rarefied flow, the shock wave is a region of finite thickness, the dimension of which depends on the transport properties of the gas. Hence, the shock wave location must be identified with some established criterion; in the present case this is chosen to be the velocity center of the shock wave, defined from the inflection point in shock-normal velocity.

Velocity is a fundamental flow property that is neither inferred nor dependent on the condition of thermal equilibrium, such as is the case for pressure and temperature. The difference in the descriptions of equilibrium and nonequilibrium flows result from differences in the thermodynamic behavior of the gas if the dynamic aspects are the same. Therefore, the location of the shock wave is referenced to the normal velocity profile (η direction in Fig. 2).

Normal velocity profiles along the stagnation streamline and their dependence on the power law exponent are shown in Fig. 3. Each profile has been taken through cell centroids that lie very close to the stagnation line and, therefore, can be considered as being situated along the stagnation streamline. Here η/λ_∞ is the dimensionless distance away from the body (Fig. 2). In Fig. 3, the normal velocity is expressed as a fraction of the freestream velocity. Note that each of the predictions of normal velocity for all of the power law exponents shows a gradual merging of the shock layer and shock wave; the blending becomes more gradual with decreasing power law exponent n. As n increases, the velocity profile becomes steeper indicating that the shock structure becomes thinner.

Figure 4 shows the shock wave shapes in the vicinity of the stagnation region for body power law exponents of $\frac{1}{2}$, 0.6, $\frac{2}{3}$, 0.7, $\frac{3}{4}$, and 0.8. In Fig. 4, X and Y are the length x and height y normalized by

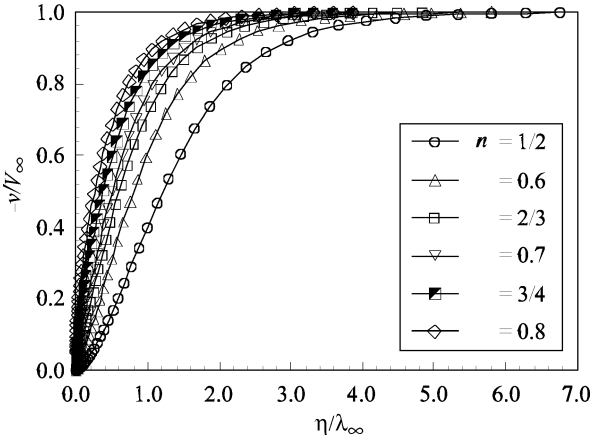

Fig. 3 Dimensionless normal velocity profiles along the stagnation streamline for various power law bodies.

the freestream mean free path λ_∞. Note that each coordinate point in the shock wave shape corresponds to the inflection point in the normal velocity profiles in the η direction, calculated for several stations along the body surface.

Interesting features can be observed in Fig. 4. In the $n = 0.8$ case, shown in Fig. 4f, the shock wave shape begins just above the leading edge and does not cross the stagnation streamline ahead of the leading edge. Farther downstream from the leading edge, the shock wave seems to be straight indicating a wedgelike structure, similar to the shape found by Oguchi[21] near the leading edge of a sharp flat plate. Afterward, the complete solution shows the shock wave changing continuously from a wedgelike structure to a power law structure, that is, following the body shape, as will be shown later. As the power law exponent decreases from 0.8 to $\frac{2}{3}$, the position of the shock wave moves upstream on the body, the straight part of the shock wave diminishes, indicating that the bluntness effect becomes significant. Still decreasing the power law exponent, the shock wave jumps ahead of the leading edge, crossing the stagnation streamline. The wedgelike structure disappears, and the shock wave shape approaches the parabolic one, as will be shown subsequently.

It was pointed out by Lees and Kubota[3] that flow similarity is possible for a class of bodies of the form x^n. In the more general case for $0 < n < 1$, the shock wave grows as x^m. When n grows from zero, m begins by keeping the constant value $m = 2/(j+3)$, and if n keeps on growing toward unity, m remains equal to n. Here j takes the values zero for planar flow and one for axisymmetric flow.

The classic hypersonic similarity solutions are obtained with a slender-body approximation. Consequently, they should not be valid near the nose of the leading edge, where this slender-body approximations are violated. At or near the nose, the surface slope, the curvature, and the higher derivatives are infinite; therefore, the similarity solutions should break down, and it is not clear that the similarity arguments can be applied to define shock shape. To evaluate this, a fitting process has been performed over the coordinate points, shown in Fig. 4, to approximate the shock wave shapes as a power law curve of the following form:

$$y = A(x + B)^m \tag{2}$$

where A is the power law constant of the curve fit, B is the distance from the nose of the leading edge, and m is the power law exponent of the curve fit, that is, the shock wave power law exponent.

To compare the shock wave shapes obtained in this work with those predicted by Lees and Kubota,[3] curve-fit solutions are found by keeping $m = \frac{2}{3}$ for $n \leq \frac{2}{3}$ cases and $m = n$ for $n > \frac{2}{3}$ cases, where n and m are body and shock wave power law exponents, respectively. Moreover, based on the shock wave shapes in Fig. 4, the whole domain is separated into two regions: an inner region defined by $X(\equiv x/\lambda_\infty) \leq 3.0$, where the bluntness effects are assumed to be dominant, and an outer region from this point to the end of the leading edge, where the bluntness effects are supposed to be negligible. The boundary of these regions was defined by visual inspection. In this context, the fitting process is performed over the points yielded by DSMC simulations, located in the outer region, where it is expected that the blunt nose effects are not significant. Recall that the shock wave shape in the inner region is not correctly predicted by the theoretical solutions, because the hypersonic slender-body approximations are violated close to or at the nose of the leading edges as already explained.

Figure 5 shows the shock wave shape solution in the outer region for a body power law exponent of $\frac{2}{3}$, the limiting case in which it is expected that the shock wave would grow with $x^{2/3}$. In Fig. 5, n and m are the body and shock wave power law exponents, respectively. As can be seen, the DSMC solution presents excellent agreement with the analytical solution of the hypersonic slender-body approximations. Moreover, the curve-fitted solution deviates from the DSMC solution close to the nose of the leading edge, as would be expected.

Figure 6 shows the shock wave solutions in the outer region for a body power law exponent of 0.6. For this body power law case, two curve-fit solutions are investigated, $m = 0.6$ and $\frac{2}{3}$. Observe from Fig. 6 that the shock wave shape given by $m = \frac{2}{3}$ presents better agreement with the DSMC solution than that yielded by $m = 0.6$.

The shock wave solutions in the outer region for a body power law exponent of $\frac{1}{2}$ are demonstrated in Fig. 7. Similar to the preceding case, two curve-fit solutions are also investigated for this body power law, $m = \frac{1}{2}$ and $\frac{2}{3}$. As can be seen, having the shock wave grow with $x^{2/3}$ provides better agreement than a fit to $x^{1/2}$, even though the body grows as $x^{1/2}$.

By the comparison of the curve-fit solutions shown in Figs. 5–7, it is observed that the region where the solutions do not match, that is, in the vicinity of the nose of the leading edges, increases as the body power law exponent decreases. By decreasing the body power law exponent, the bluntness effect becomes more pronounced and the shock wave shapes depend more on the details of the nose geometry. Also note from Figs. 5–7 that, along the stagnation streamline, the solutions given by $m = \frac{2}{3}$ overpredict the shock wave detachment distance, whereas the solutions given by $m = n$ underpredict it, as compared to the DSMC solutions. Overall, for values of $\frac{1}{2} \leq n \leq \frac{2}{3}$, the best agreement to DSMC solutions in the outer region ($X > 3.0$) is found with shock wave shapes that are scaled to $x^{2/3}$. This result is in agreement with the similarity solutions predicted by Lees and Kubota.[3]

The shock wave shapes in the outer region for body power law exponents of 0.7, $\frac{3}{4}$, and 0.8 are presented in Figs. 8–10, respectively. Figures 8–10 show comparisons of the results obtained by the fitting process with those yielded by the DSMC simulations. It can be seen that the DSMC results are closely matched by the results predicted by the theoretical solutions, that is, the shock wave shape follows the body shape. Note that in these cases no smoothing process has been applied to the points describing the DSMC curves.

A new form of the curve fit is considered in defining the shock wave shape in the inner region, $X \leq 3.0$. In this region, A, B, and m in Eq. (2) are found by the fitting process for body power law exponents of $\frac{1}{2}$ and 0.6. Another solution investigated was keeping $m = \frac{1}{2}$ or 0.6 and finding A and B by the fitting process.

Table 3 presents the results for power law constants A and B and power law exponent m, obtained only for body power law exponents of $\frac{1}{2}$ and 0.6. The power law constant A has the dimension of $\mathrm{m}^{1-\mathrm{m}}$, and constant B is normalized by the freestream mean free path λ_∞.

Figure 11 shows the comparison between the solutions of this new form of the curve fit and those yielded by the DSMC simulations, for

Table 3 Curve-fit power law exponents and curve-fit constants

Exponent n	Exponent m	Constant A	Constant B
$\frac{1}{2}$	0.5	0.09962	0.78467
$\frac{1}{2}$	0.531	0.11928	0.79155
0.6	0.5	0.08011	0.42161
0.6	0.526	0.09534	0.42691
0.6	0.6	0.15484	0.43583

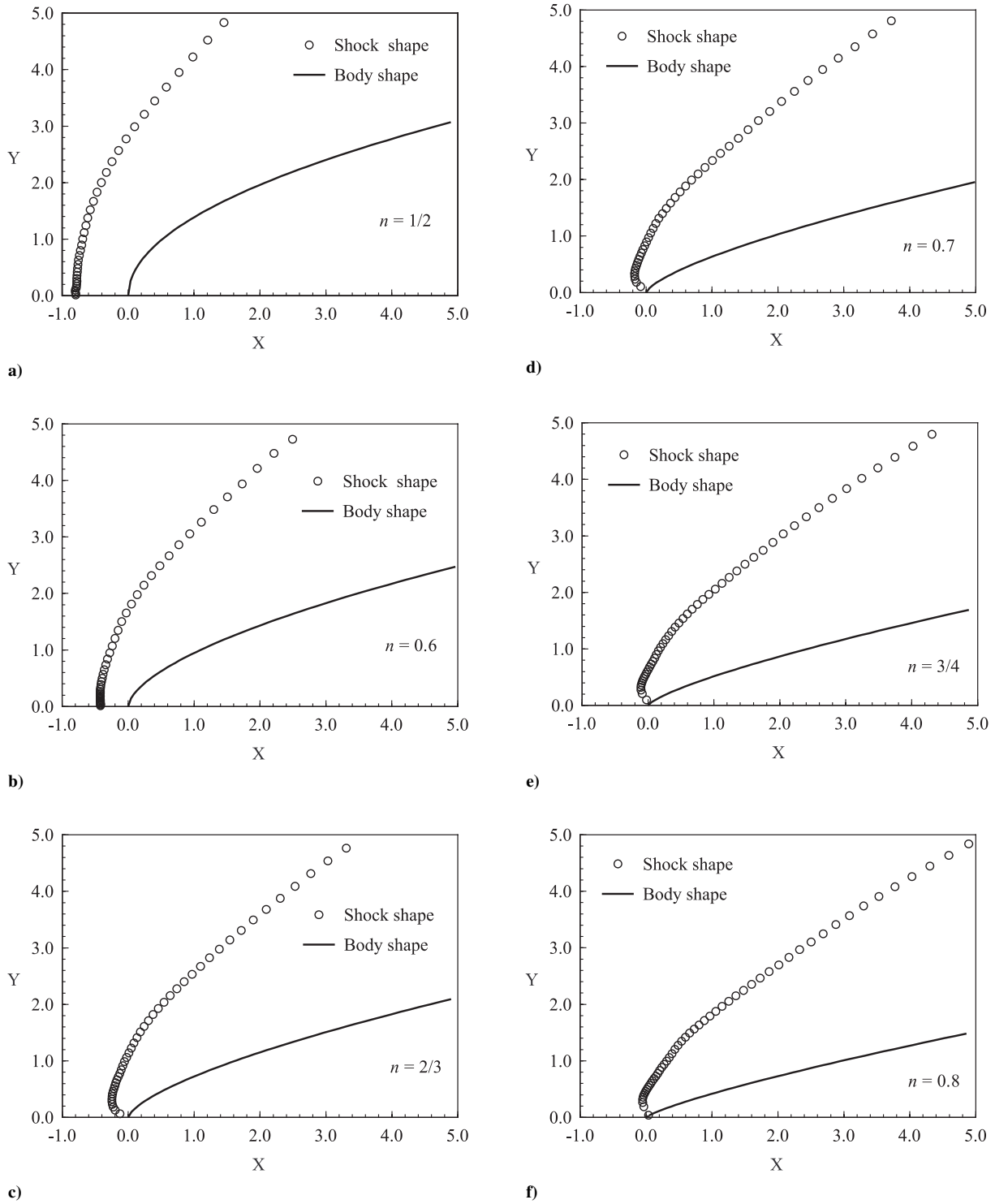

Fig. 4 Shock wave shapes on various power law body shapes: a) $n = \frac{1}{2}$, b) $n = 0.6$, c) $n = \frac{2}{3}$, d) $n = 0.7$, e) $n = \frac{3}{4}$, and f) $n = 0.8$.

body power law exponent of $\frac{1}{2}$. As shown in Fig. 11, the curve-fit solutions do not yield a power law exponent m that closely reproduces the DSMC solutions in the inner region. Near the stagnation streamline, the shock wave shape given by $m = \frac{1}{2}$ offers better agreement to the DSMC. This behavior is brought out more clearly in Fig. 11b, which exhibits details of the shock wave curve fits near the stagnation streamline.

In an effort to provide additional qualitative information, the shock wave shape for body power law exponent of $\frac{1}{2}$ as found by the DSMC simulations is compared to the parabolic shock wave shape obtained by the thin shock wave theory, valid in hypersonic continuum flow. The shape of the parabolic shock wave[22] is given by $y = \sqrt{(2R_c x)}$, where R_c is the radius of curvature at the nose of the leading edge. This relation is obtained by assuming that the shock wave lies on the origin of the coordinate system. The radius of curvature at the nose of the leading edge for the $n = \frac{1}{2}$ case, obtained from the general formula for the longitudinal radius of curvature,[20] is simply by $a^2/2$, where a is the body power law constant defined in Eq. (1). Hence, the relation for the parabolic shock wave reduces to $y = a\sqrt{x}$. When this expression is compared with that given by Eq.(2) with $m = \frac{1}{2}$, and when it is considered that the body power law constant a [Eq. (1)] and the curve-fit power law constant A [Eq. (2)] are different for body power law exponent of $\frac{1}{2}$, the thin shock-wave theory fails to reproduce the parabolic shock wave

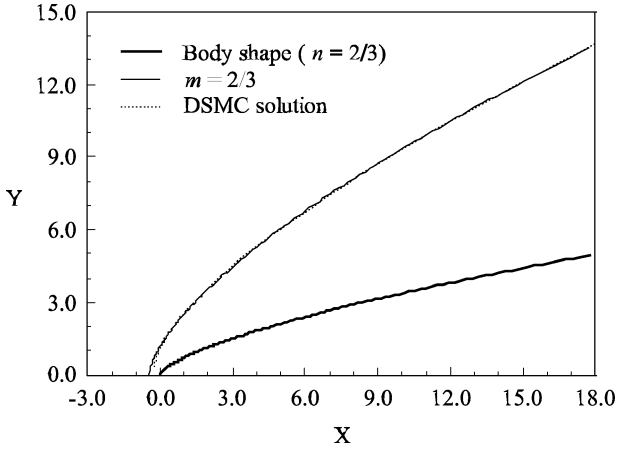

Fig. 5 Shock wave shape curve fits on $n = \frac{2}{3}$ body shape in the outer region.

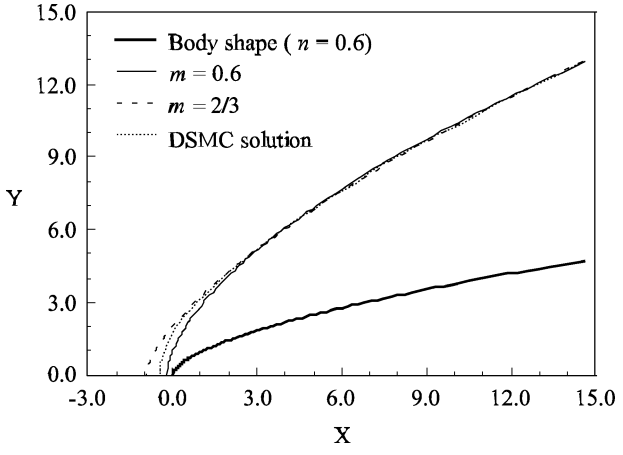

Fig. 6 Shock wave shape curve fits on $n = 0.6$ body shape in the outer region.

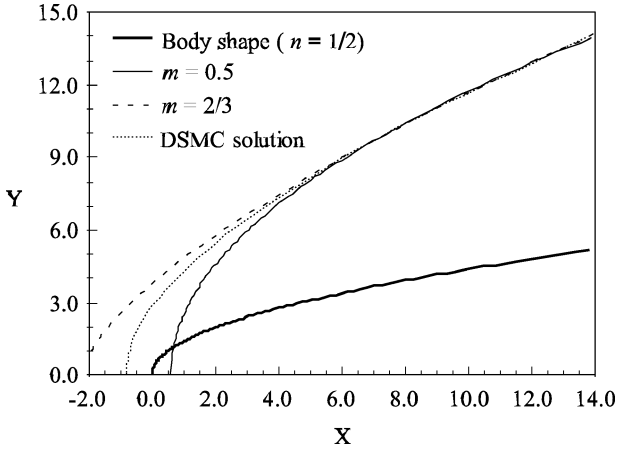

Fig. 7 Shock wave shape curve fits on $n = \frac{1}{2}$ body shape in the outer region.

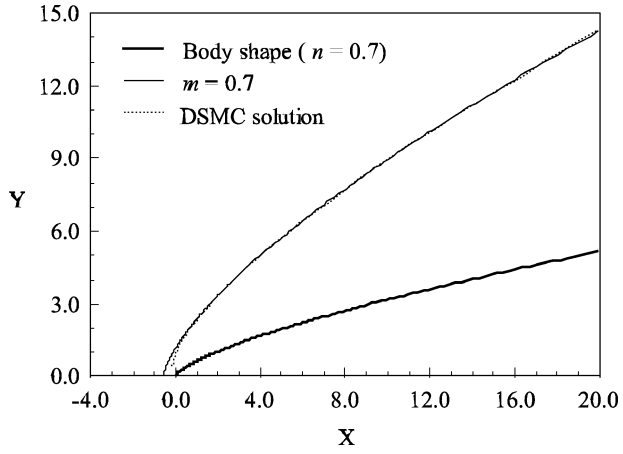

Fig. 8 Shock wave shape curve fits on $n = 0.7$ body shape in the outer region.

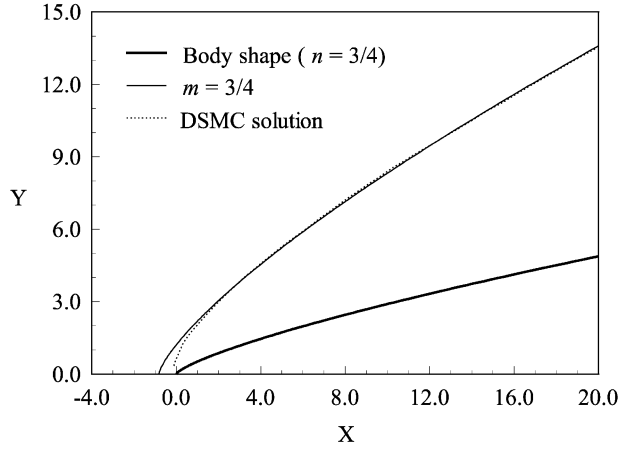

Fig. 9 Shock wave shape curve fits on $n = \frac{3}{4}$ body shape in the outer region.

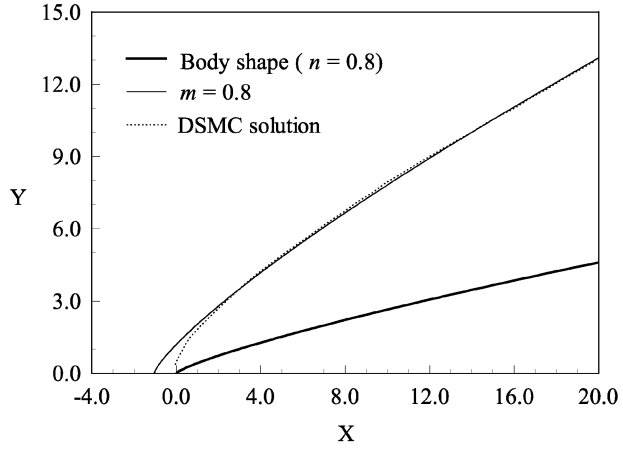

Fig. 10 Shock wave shape curve fits on $n = 0.8$ body shape in the outer region.

(Fig. 11) in rarefied hypersonic flow. Thin shock wave theory makes an assumption of constant density in the viscous shock layer, but this assumption does not hold for cold-wall flows.[23] As a point of reference, the wall-to-stagnation temperature ratio (T_w/T_0) for this work was set to 0.13.

Figure 12 shows the comparison of the shock wave curve fits and the results of the DSMC simulations for a body power law exponents of 0.6. As shown in Fig. 12, the shock wave curve-fit solutions given by $m = 0.5$ and 0.526 offer close agreement with the DSMC results near the stagnation region, but deviate from them at the end of the domain where the solutions were computed. A possible explanation for this behavior might be found in the size of the inner region defined earlier. The exhibited results seem to indicate that the inner region should be larger than $3\lambda_\infty$ as $n \to \frac{1}{2}$ and smaller than that as $n \to 0.8$. This is more evident in Figs. 5 and 7, where the curve fit obtained for the outer region still presents a good agreement in a significant portion of the inner region. Referring to Fig. 12, it is also observed that the shock wave curve fit given by $m = 0.6$ diverges from the shock wave predicted by the DSMC simulations at the end of the inner region. For comparison purpose, a magnified view

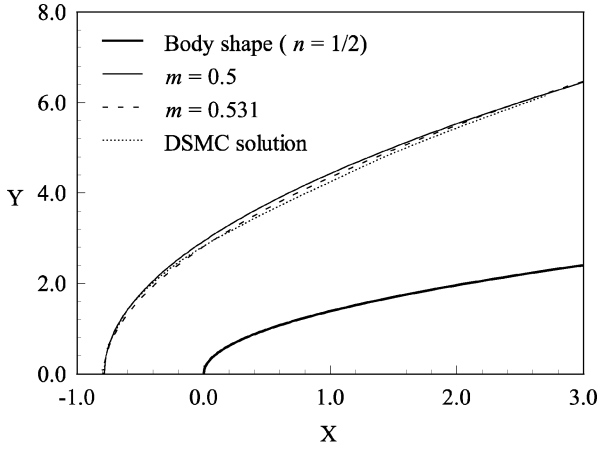

a) Full view

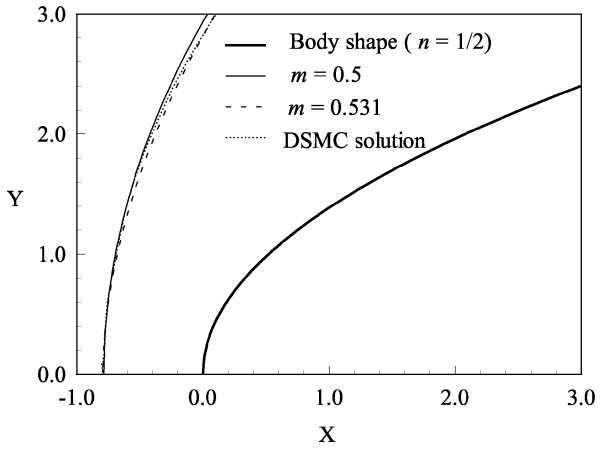

b) Magnified view

Fig. 11 Shock wave shape curve fits on $n = \frac{1}{2}$ body shape in the inner region.

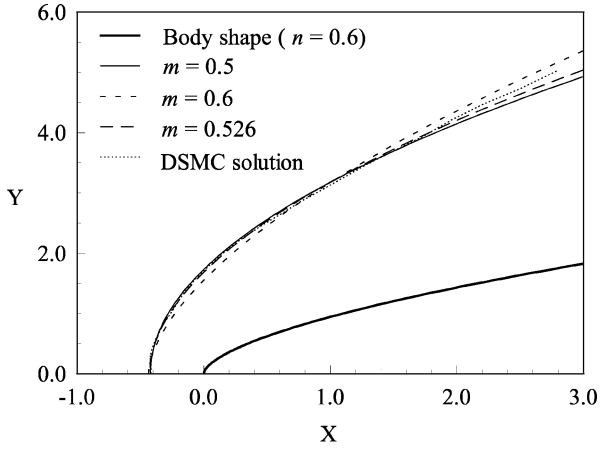

a) Full view

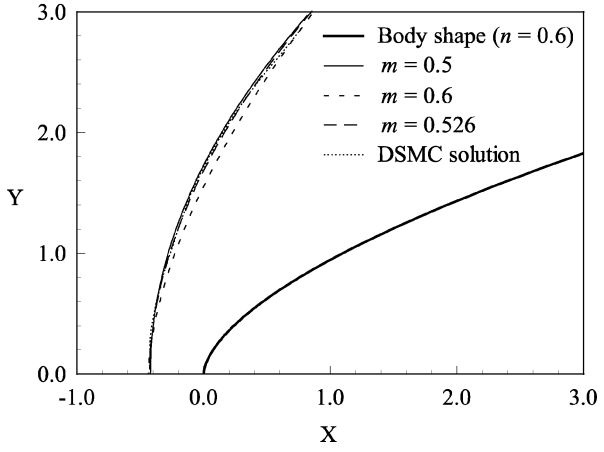

b) Magnified view

Fig. 12 Shock wave shape curve fits on $n = 0.6$ body shape in the inner region.

of the shock wave shapes close to the stagnation region for body power law exponent of 0.6 is shown in Fig. 12b. From Fig. 12b, it is seen that shock wave shapes given by $m = 0.5$ and 0.526 offer better agreement, as compared to that predicted by DSMC simulations. No attempt was made to define the shock wave shapes in the inner region for body power law exponents $n \geq \frac{2}{3}$, because the shock waves do not cross the stagnation streamline ahead of the leading edge for these cases (Fig. 4).

It is well known that the curved shock wave supported by a blunt-nosed body introduces vorticity in the flowfield between the body and the shock wave. From the analytical solution for continuum flow,[22] the vorticity immediately behind a curved shock wave is given by

$$\Omega = V_\infty \frac{\rho_2}{\rho_\infty}\left(1 - \frac{\rho_2}{\rho_\infty}\right)^2 \cos\beta \frac{\mathrm{d}\beta}{\mathrm{d}s} \tag{3}$$

where ρ_2 is the density immediately behind the shock wave. Once again, the shock wave lies on the origin of the coordinate system.

When Eq. (2) with $B = 0$ and the definition of the arc length s along the cosine of the angle are used, Eq. (3) reduces to

$$\Omega = V_\infty \frac{\rho_2}{\rho_\infty}\left(1 - \frac{\rho_2}{\rho_\infty}\right)^2 \frac{m(m-1)Ax^{m-2}}{(1 + m^2A^2x^{2m-2})^2} \tag{4}$$

In the limit of small x, the vorticity is approximated by the following expression:

$$\Omega \simeq V_\infty \frac{\rho_2}{\rho_\infty}\left(1 - \frac{\rho_2}{\rho_\infty}\right)^2 \frac{(m-1)Ax^{2-3m}}{m^3A^3} \tag{5}$$

In the limit as $x \to 0$, the vorticity behind a power law shock wave approaches minus infinity for power law exponents $m > \frac{2}{3}$. By the analysis of the DSMC results for the shock wave shapes, it can be observed that the power law exponents m are less than $\frac{2}{3}$ for body power law exponents given by $n < \frac{2}{3}$. However, as $n \geq \frac{2}{3}$, the shock wave shapes are no longer described by a power law as $x \to 0$. This might be an indication that the solutions are avoiding the infinity vorticity that would be immediately behind a power law shock wave with $n \geq \frac{2}{3}$. Therefore, the qualitative findings regarding vorticity in the continuum regime seem to hold for the direct simulation results investigated here. This finding was also observed by O'Brien,[24] when the shock wave shape of power law leading edges was investigated by assuming two-dimensional, inviscid, and perfect gas conditions.

Overall, no unique power law exponent has been found that describes the shock wave shape in the total length of the leading edges investigated. The results indicate that each of the shock wave shapes is best represented by two power law exponents m. One of these is applied to the region near the nose of the leading edge, where the effects of the blunt nose are important. The other one represents the region where the nose blunt effects are no longer important, as predicted by the classical analytical solution.

One of the most surprising results in this work is that the shock wave shapes near the stagnation region for leading edges given by power law exponents of $\frac{1}{2}$ and 0.6 are both represented by m close to $\frac{1}{2}$, as shown in Figs. 11b and 12b. The examples of Refs. 10–12 represent flows at conditions and geometries that are very different than the ones chosen here, but they found a tendency toward parabolic shock waves. This supports the conclusion that the exponent of $\frac{1}{2}$ is preferred for the shock wave shape near the stagnation streamline for blunt bodies.

Shock Wave Thickness

In a rarefied flow, the shock wave is a finite region that depends on the transport properties of the gas. As such, the effect of the power law body shape on the shock wave thickness has been calculated with the DSMC solutions. The shock wave thickness is defined again with the maximum-slope definition of shock thickness: for a given property ϕ, which may be velocity, temperature, density, or pressure, the thickness is defined in a dimensional form in the shock-normal direction[25] by

$$\delta = \frac{\phi_{\max} - \phi_{\min}}{|\mathrm{d}\phi/\mathrm{d}\eta|_{\max}} \tag{6}$$

where the maximum and minimum values of ϕ occur at $\eta = \pm\infty$. The term $|\mathrm{d}\phi/\mathrm{d}\eta|_{\max}$ represents the absolute value of the maximum gradient of ϕ, regardless of the location within the shock wave where it occurs. The spatial coordinate is η. Note that, because each physical variable will have its own profile, each one would also have its own characteristic thickness. Therefore, the definition of thickness of a shock wave depends on the quantity ϕ that is being measured. Grad[26] as well as Gilbarg and Paolucci[27] have emphasized that an objection to the definition given by Eq. (6) is that it depends on a purely local feature of the shock wave profile and that in the general case this measure of shock thickness is unrealistically small.

The shock wave thickness in the present work is obtained from velocity. With reference to Eq. (6), $\phi_{\max}$ is the velocity upstream of the shock and $\phi_{\min}$ the velocity downstream of the shock along the stagnation streamline. The first derivative is obtained from the velocity profile curve fit. In dimensionless form, the upstream velocity $\phi_{\max}(= v/V_\infty)$ is defined as being 0.99 and the downstream velocity $\phi_{\min}$ as 0.01.

The inflection points in the normal velocity profile have been employed to determine an approximate shock wave center for each of the body power law shapes. The normal case does not include the complicating effect of molecular interactions with solid surfaces. Note that some velocity profiles in the present work have no inflection point in the along the stagnation streamline. As was shown in Fig. 2, there is a difference in the velocity profile behavior for $n < \frac{2}{3}$ from that for $n \geq \frac{2}{3}$. It is seen that the velocity profile presents a nearly linear shape close to the nose of the leading edge for $n = \frac{2}{3}$. For $n < \frac{2}{3}$, there are inflection points for the cases investigated. However, there are no inflection points for cases corresponding to $n \geq \frac{2}{3}$.

Because of the lack of inflection point in the normal velocity profile along the stagnation streamline for body power law with $n \geq \frac{2}{3}$, the shock wave thickness is assumed to be the distance from the nose of the leading edge (stagnation point) to the point that corresponds to $\phi_{\max}$ measured along the stagnation streamline.

The shock wave thickness δ obtained by the two processes normalized by the freestream mean free path λ_∞ is presented in Table 4. For comparison, the shock wave thickness for the tangent circular cylinder to which the power law shapes are referenced (Fig. 1) is also presented in Table 4. It is seen from Table 4 that the shock wave thickness given by Eq. (6) increases dramatically, around 88%, as the leading edge changes from power law to the circular cylinder. Because the shock wave thickness is estimated by $\phi_{\max}$, a significant decrease is observed in the thickness when the leading edge changes from blunt ($n = \frac{1}{2}$) to sharp ($n = 0.8$).

Table 4 Computational results for dimensionless shock wave thickness δ/λ_∞

Exponent n	Eq. (6)	Shock thickness, $\phi_{\max}$
$\frac{1}{2}$	1.991	5.011
0.6	1.427	3.936
$\frac{2}{3}$	——	3.386
0.7	——	3.070
$\frac{3}{4}$	——	2.795
0.8	——	2.484
Cylinder	3.712	7.239

Table 5 Dimensionless shock wave detachment distance Δ/λ_∞

Exponent n	Exponent m	DSMC solution	Constant B
$\frac{1}{2}$	——	0.795	——
$\frac{1}{2}$	0.5	——	0.785
$\frac{1}{2}$	0.531	——	0.792
0.6	——	0.420	——
0.6	0.5	——	0.422
0.6	0.526	——	0.427
0.6	0.6	——	0.436
Cylinder	——	2.755	——

Shock Wave Detachment Distance

The shock wave detachment distance Δ, defined as the distance between the shock wave center and the nose of the leading edge, measured along the stagnation streamline, is presented in Fig. 4. In general, it is seen that the shock detachment distance decreases as n increases, as would be expected.

A quantitative comparison of the shock wave detachment distance, given by the inflection point in the velocity profile, normalized by the freestream mean free path λ_∞, is presented in Table 5. Table 5 also presents the shock wave detachment distance for the curve-fitted shock waves obtained by the constant B in Eq. (2).

With reference to Table 5, note that the blunter the leading edge is the larger the shock wave detachment distance. The shock wave detachment distance for the circular cylinder is significantly larger than that for the power law shape defined by the $n = \frac{1}{2}$ case. Furthermore, the shock wave detachment decreased by almost 50% as the leading edge shape changed from $\frac{1}{2}$ to 0.6.

The shock-wave detachment distance is especially important in hypersonic vehicles such as waveriders, which depend on leading-edge shock attachment to achieve their high lift-to-drag ratio at high lift coefficient. In this context, the power law leading edges seem to be more appropriate than the circular cylinder, because they present reduced shock wave detachment distances. Nevertheless, smaller shock detachment distance is associated with a higher heat load to the nose of the body.[8]

Conclusions

This study applies the DSMC method to assess the impact on the shock wave structure due to variations in the shape of power law leading edges. The calculations have provided information concerning the nature of the shock wave shape, shock thickness, and shock wave detachment distance resulting from variations in the body shape for the idealized situation of two-dimensional hypersonic rarefied flow.

The computational results indicated that the shock wave shape grows with power law forms x^m for power law leading edges. It was found that the shock wave shape is best represented by two exponents m that describe two separate regions for the majority of the power law leading edges investigated. One exponent m applies to the region near the nose of the leading edges (inner region), where the effects of bluntness are important. The other exponent m describes the shock wave far from the nose (outer region), where the blunting effects are of reduced significance.

The calculated shape of the shock wave in the so-called outer region is matched well by the predictions of hypersonic small disturbance theory in that the shape of the shock wave follows the shape of the body, provided the body power law exponent is larger than $\frac{2}{3}$. In the inner region, in the vicinity of the nose, the shock wave shape is better represented by $m = \frac{1}{2}$ regardless of exact nose shape.

Appendix: Grid Validation

This section focuses on the analysis of the influence of the cell size and the number of particles per computational cell on the surface properties to achieve grid-independent solutions. In the DSMC algorithm, the cell size has to be less than the local mean free path, and the number of simulated particles has to be large enough to make the statistical correlations between particles insignificant.[28]

The analysis is limited to the $n = \frac{1}{2}$ case. The same procedure was adopted for the other cases.

Effect of Grid Variation

The effect of grid resolution on computed results is of particular interest for the present study because insufficient grid resolution[29] can reduce significantly the accuracy of the predicted aerodynamic heating and forces acting on the body surface. Hence, heat transfer, pressure, and skin-friction coefficients are used as the representative parameters for the grid sensitivity study.

The effect of altering the size of the computational cells is investigated for a series of three simulations with structured grids of 35 (coarse), 70 (standard), and 105 (fine) cells in the ξ direction and 50 cells in the η direction (Fig. 2). Each grid was made up of nonuniform cell spacing in both directions. The effect of changing the number of cells in the ξ direction is shown in Fig. A1 as it impacts the calculated skin friction, heat transfer and pressure coefficients. The comparison shows that the calculated results are rather insensitive to the range of cell spacing considered.

In analogous fashion, an examination was made in the η direction. The sensitivity of the calculated results to cell size variations in the η direction is shown in Fig. A2 for the skin-friction, heat transfer, and pressure coefficients. In Fig. A2, a new series of three simulations with grid of 70 cells in the ξ direction and 25 (coarse), 50 (standard) and 75 (fine) cells in the η direction is compared. The cell spacing in both directions is again nonuniform. According to Fig. A2, the results for the three grids are approximately the same, indicating that the standard grid, 70×50 cells, is essentially grid independent. For the standard case, the cell size in the η direction is always less than the local mean free path length in the vicinity of the surface.

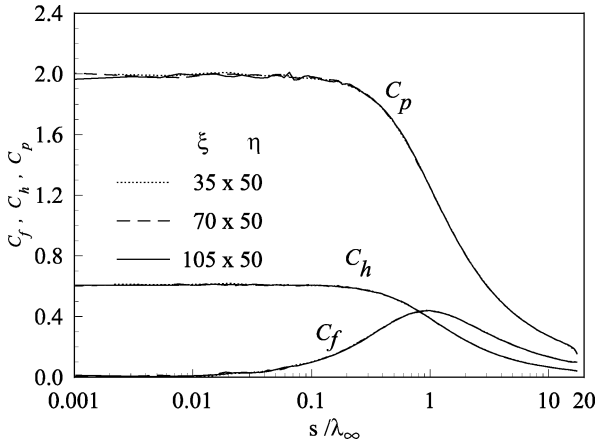

Fig. A1 Effect of altering cell size in the ξ direction on skin friction, heat transfer, and pressure coefficients.

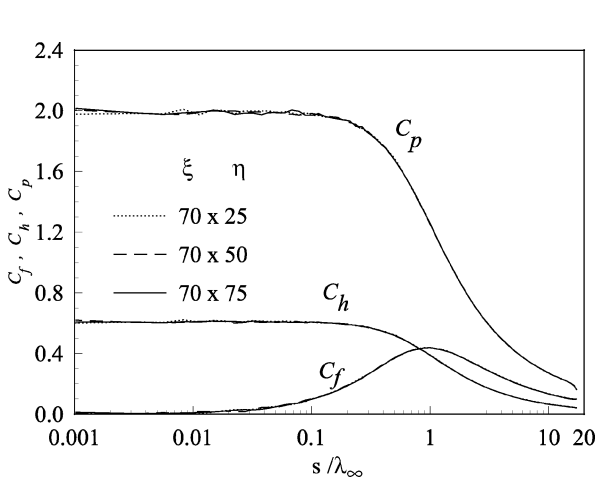

Fig. A2 Effect of altering cell size in the η direction on skin friction, heat transfer, and pressure coefficients.

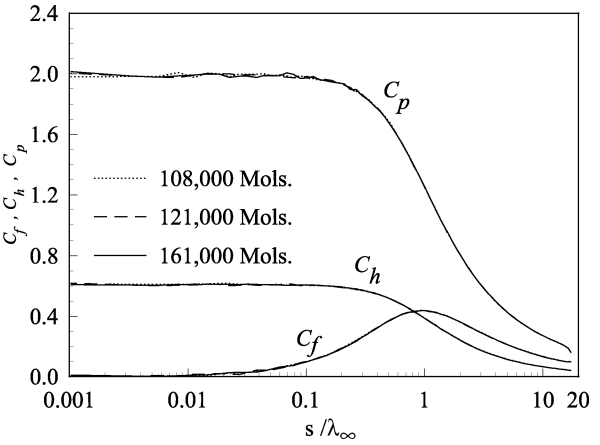

Fig. A3 Effect of altering number of molecules on skin friction, heat transfer, and pressure coefficients.

Effect of Number of Molecules

The number of simulated molecules is a crucial parameter for any DSMC study. There should be enough molecules in the simulation so that the statistical correlations do not affect the result of the simulation. In this context, a similar examination was made for the number of molecules. The sensitivity of the calculated results to number of molecule variations is shown in Fig. A3 for skin-friction, heat transfer, and pressure coefficients. The standard grid, 70×50 cells, corresponds to a total of 121,000 molecules. Two new cases using the same grid were investigated. These new cases correspond to, on average, 108,000 and 161,000 molecules in the entire computational domain. It is seen that the standard grid with a total of 121,000 molecules is enough for the computation of the aerodynamic surface quantities.

References

[1]Nonweiler, T. R. F., "Aerodynamic Problems of Manned Space Vehicles," *Journal of the Royal Aeronautical Society*, Vol. 63, Sept. 1959, pp. 521–528.

[2]Van Dyke, M. D., "A Study of Hypersonic Small-Disturbance Theory," NACA TN-3173, 1954.

[3]Lees, L., and Kubota, T., "Inviscid Hypersonic Flow over Blunt-Nosed Slender Bodies," *Journal of Aeronautical Sciences*, Vol. 24, No. 3, 1957, pp. 195–202.

[4]Freeman, N. C., Cash, R. F., and Bedder, D., "An Experimental Investigation of Asymptotic Hypersonic Flows," *Journal of Fluid Mechanics*, Vol. 18, No. 3, 1964, pp. 379–384.

[5]Beavers, G. S., "Shock-Wave Shapes on Hypersonic Axisymmetric Power-Law Bodies," *AIAA Journal*, Vol. 7, No. 10, 1969, pp. 2038–2040.

[6]Hornung, H. G., "Some Aspect of Hypersonic Flow over Power Law Bodies," *Journal of Fluid Mechanics*, Vol. 39, No. 1, 1969, pp. 143–162.

[7]Mason, W. H., and Lee, J., "Aerodynamically Blunt and Sharp Bodies," *Journal of Spacecraft and Rockets*, Vol. 31, No. 3, 1994, pp. 378–382.

[8]Santos, W. F. N., and Lewis, M. J., "Power Law Shaped Leading Edges in Rarefied Hypersonic Flow," *Journal of Spacecraft and Rockets*, Vol. 39, No. 6, 2002, pp. 917–925.

[9]Santos, W. F. N., and Lewis, M. J., "Angle of Attack Effect on Rarefied Hypersonic Flow over Power Law Shaped Leading Edges," *Proceedings of the 23rd International Symposium on Rarefied Gas Dynamics*, edited by A. D. Ketsdever and E. P. Muntz, Vol. 663, AIP Conf. Proceedings, New York, 2003.

[10]Vas, I. E., Bogdonoff, S. M., and Hammitt, A. G., "An Experimental Investigation of the Flow over Simple Two-Dimensional and Axial Symmetric Bodies at Hypersonic Speeds," *Jet Propulsion*, Vol. 28, No. 2, 1958, pp. 97–104.

[11]McCarthy, J. F., and Kubota, T., "A Study of Wakes Behind a Circular Cylinder at $M = 5.7$," *AIAA Journal*, Vol. 2, No. 4, 1964, pp. 629–636.

[12]Zapata, R. N., Haas, J., and Mruk, G. K., "Low Reynolds Number Effects on Hypersonic Flow over a Two-Dimensional Cylinder," *Advances in Applied Mechanics*, Vol. 2, Suppl. 4, 1967, pp. 1161–1176.

[13]Bird, G. A., *Molecular Gas Dynamics and the Direct Simulation of Gas Flows*, Oxford Univ. Press, Oxford, 1994.

[14]Hadjiconstantinou, N. G., "Analysis of Discretization in the Direct Simulation Monte Carlo," *Physics of Fluids*, Vol. 12, No. 10, 2000, pp. 2634–2638.

[15]Garcia, A. L., and Wagner, W., "Time Step Truncation Error in Direct Simulation Monte Carlo," *Physics of Fluids*, Vol. 12, No. 10, 2000, pp. 2621–2633.

[16]Bird, G. A., "Monte Carlo Simulation in an Engineering Context," *Rarefied Gas Dynamics*, edited by Sam S. Fisher, Vol. 74, Progress in Astronautics and Aeronautics, Pt. 1, AIAA New York, 1981, pp. 239–255.

[17]Borgnakke, C., and Larsen, P. S., "Statistical Collision Model for Monte Carlo Simulation of Polyatomic Gas Mixture," *Journal of Computational Physics*, Vol. 18, No. 4, 1975, pp. 405–420.

[18]Alexander, F. J., Garcia, A. L., and Alder, B. J., "Cell Size Dependence of Transport Coefficient in Stochastic Particle Algorithms," *Physics of Fluids*, Vol. 10, No. 6, 1998, pp. 1540–1542.

[19]Alexander, F. J., Garcia, A. L., and Alder, B. J., "Erratum: Cell Size Dependence of Transport Coefficient in Stochastic Particle Algorithms," *Physics of Fluids*, Vol. 12, No. 3, 2000, pp. 731–731.

[20]Santos, W. F. N., "Direct Simulation Monte Carlo of Rarefied Hypersonic Flow on Power Law Shaped Leading Edges," Ph.D. Dissertation, Dept. of Aerospace Engineering, Univ. of Maryland, College Park, MD, Dec. 2001.

[21]Oguchi, H., "The Sharp Leading Edge Problem in Hypersonic Flow," *Advances in Applied Mechanics*, Vol. 1, Suppl. 1, 1961, pp. 501–524.

[22]Rasmussen, M., *Hypersonic Flow*, Wiley, New York, 1994, pp. 36–39.

[23]Mikhailov, V. V., Neiland, V. Y., and Sychev, V. V., "The Theory of Viscous Hypersonic Flow," *Annual Review of Fluid Mechanics*, Vol. 3, Jan. 1971, pp. 371–396.

[24]O'Brien, T. F., "Analysis of Power Law Shaped Leading-Edge for Waveriders Designed with Shock Attachment," M.S. Thesis, Dept. of Aerospace Engineering, Univ. of Maryland, College Park, MD, Aug. 1998.

[25]Vincenti, W. G., and Kruger, C. H., *Introduction to Physical Gas Dynamics*, Krieger Malabar, FL, 1986.

[26]Grad, H., "The Profile of a Steady Plane Shock Wave," *Communications on Pure and Applied Mathematics*, Vol. 5, No. 3, 1952, pp. 257–300.

[27]Gilbarg, D., and Paolucci, D., "The Structure of Shock Waves in the Continuum Theory of Fluids," *Archive for Rational Mechanics and Analysis*, Vol. 2, 1953, pp. 617–642.

[28]Hadjiconstantinou, N. G., Garcia, A. L., Bazant, M. Z., and He, G., "Statistical Error in Particle Simulations of Hydrodynamic Phenomena," *Journal of Computational Physics*, Vol. 187, No. 1, 2003, pp. 274–297.

[29]Haas, B. L., and Fallavollita, M. A., "Flow Resolution and Domain Influence in Rarefied Hypersonic Blunt-Body Flows," *Journal of Thermophysics and Heat Transfer*, Vol. 8, No. 4, 1994, pp. 751–757.

I. Boyd
Associate Editor